Geophys. J. R. astr. Soc. (1983) **75**, 101–124

Calculation of complete theoretical seismograms in vertically varying media using collocation methods

Paul Spudich *U. S. Geological Survey, 345 Middlefield Road, MS77, Menlo Park, CA 94025, USA*

Uri Ascher *Department of Computer Science, University of British Columbia, Vancouver, British Columbia V6T 1W5, Canada*

Received 1983 February 4; in original form 1982 September 2

Summary. We present a method for calculating complete theoretical seismograms in earth models whose velocity, density and attenuation profiles are arbitrary piecewise-continuous functions of depth only. A form of attenuation valid for low loss situations is included by allowing the seismic velocities to be complex, and frequency is also allowed to be complex to avoid wrap-around problems in the time-domain seismograms. Solutions for the stress-displacement vectors in the medium are expanded in terms of orthogonal cylindrical functions. A seismic source is applied at the Earth's surface and a radiation condition is applied at depth. The resulting two-point boundary value problem for the expansion coefficients is solved by a collocation technique which works best for those cases that other methods, e.g. propagator matrices, work most poorly, i.e. highly evanescent solutions. Solutions for the expansion coefficients are obtained in the depth, frequency and horizontal wavenumber domain. Phase velocity filtering may be effected at this point by restricting the portion of the frequency–wavenumber plane in which solutions are sought. The transformed strain tensor at depth is formed by taking linear combinations of the solutions. This strain tensor is transformed back into the space and time domain by successive application of a Bessel transform, a fast Fourier transform, and by multiplication of the time signal by a growing exponential to remove the exponential decay introduced by the use of complex frequency. The strain tensor is contracted with a seismic moment tensor, and a reciprocity relation for Green's functions is used to obtain displacements at the Earth's surface caused by a buried moment tensor source.

1 Introduction

The calculation of theoretical seismograms in a medium in which material properties are a function of depth only ultimately reduces to the solution of a differential equation with

boundary values specified at the Earth's surface and at some great depth. Two approaches to the problem have typically been taken. If an inhomogeneous source term is included, the theoretical seismogram is usually expressed as a double integral of differential equation solutions over frequency and horizontal wavenumber (or slowness, or angle of incidence). If no source term is included in the differential equation, the problem becomes an eigenvalue-eigenvector problem and the integral over horizontal wavenumber becomes a sum of residues at poles. In both approaches numerical difficulties have been encountered in integrating the differential equations either to obtain the secular function of the medium, the eigenfunctions, or the particular solutions to the differential equations for various frequencies and wavenumbers. These difficulties and many of their solutions are well summarized by Harvey (1981).

While much of this work has approximated the Earth's velocity structure as a stack of homogeneous layers, increased attention has been given to the solution of the differential equations when more general velocity profiles, piecewise-continuous functions, are present. Several numerically stable methods have emerged for calculating complete seismograms in piecewise-continuous velocity profiles. For eigenvalue-eigenfunction calculations the Rayleigh–Ritz procedure has been used by Wiggins (1976) and others. The recent work of Alekseev & Mikhalenko (1980) and Olson, Orcutt & Frazier (1983) has focused attention on the solution of such problems when a source is included from the outset. In their approaches, a partial differential equation in depth and time is solved by a time-stepping finite-difference or finite-element method, respectively, to obtain the stress-displacement vectors in the wavenumber, depth and time domain. The particular solutions for each wavenumber are then summed to obtain the theoretical seismograms. These methods are computationally robust and have already been used in practical applications (e.g. Hartzell & Helmberger 1982). Certain inconveniences arise from the solution of the differential equations in the time domain, however. Since time-stepping algorithms are used, calculations must always commence when the source acts, regardless of the epicentral range of the desired Green's function. Hence, at large epicentral distance, considerable computational effort is expended calculating the string of zeros preceding the initial P motion. Currently, neither time domain method includes attenuation, although a depth-dependent Q could probably be incorporated by allowing wavenumber to be a complex function of depth. However, making this attenuation frequency dependent is probably impossible. In addition, phase velocity filtering, which has proved so useful in frequency domain methods such as that of Fuchs & Müller (1971), is possible but cumbersome in the time-domain methods. For these reasons we have chosen to follow an approach similar to Olson's but in the frequency domain.

In this paper we present a method for the calculation of complete theoretical seismograms in laterally homogeneous earth models, i.e. in earth models in which seismic velocities, density and attenuative quality factor Q are functions of depth only. The strongest assets of this method are its generality, flexibility and robustness. The method is general because the velocity- and density-depth profiles may be arbitrary piecewise-continuous functions of depth. The method is flexible because it can be used in any distance range, either near field or far field, to calculate all possible body waves, surface waves and leaky modes. In addition, phase velocity and group velocity windowing can be used to calculate specific seismic phases of interest or specific time windows of interest. The robustness of the method springs from the use of a collocation technique to solve for the stress-displacement vectors as functions of depth, frequency and wavenumber. The use of this technique to solve the two-point boundary value problem for the stress-displacement vectors avoids the numerical difficulties commonly encountered when propagator matrices. Runge-Kutta integrations and other

initial value methods are employed. We shall thus refer to our method as the 'collocation seismogram method' (CSM) and refer to seismograms calculated using the CSM as 'collocation seismograms'.

The chief flaw of our current incarnation of the CSM is its long computation time, being roughly competitive with other complete theoretical seismogram methods such as the discrete wavenumber/finite element (DWFE) method of Olson *et al.* (1983). However, we do not consider this version of the CSM to be computationally optimized. In Section 4 we discuss a number of ways to improve the efficiency of the method.

First, however, we present the theory behind the CSM, emphasizing the solution of the boundary value problem using the collocation technique since its use in seismology is new. We de-emphasize the particular Bessel transform employed because any of a variety will work, although some may be considerably more efficient than others. To verify the correctness of the CSM, we show comparisons of collocation seismograms with those calculated using the DWFE method.

2 Theory

Our general plan of attack will follow that of Olson *et al.* (1983). We first find particular solutions to the boundary value problems for three orthogonal forcing terms applied at $z = 0$, the Earth's surface. We then take linear combinations of the particular solutions to obtain the solutions for orthogonal point forces applied at the Earth's surface, i.e. to obtain the Green's functions for the medium. From these Green's functions one can obtain the strain tensor in the medium, which is then contracted with the seismic moment tensor to obtain the ground displacements caused by the point moment seismic source.

Consider a half-space in which P-wave velocity, α, S-wave velocity β and density ρ are functions of depth into the half-space, z, only. In the depth interval $0 \leqslant z < z_>$ we allow $\alpha(z)$, $\beta(z)$ and $\rho(z)$ to be arbitrary piecewise-continuous functions of depth. For depths $z \geqslant z_>$, we require the wave speeds to be constant, i.e. $\alpha(z) = \alpha_>$, $\beta(z) = \beta_>$ and $\rho(z) = \rho_>$, as shown in Fig. 1. In addition, following Kennett (1975) we approximate the effects of anelastic attenuation by allowing α and β to be complex functions of depth. In our current version of the method, we set

$$\begin{aligned} \mathrm{Im}\,[\alpha(z)] &= \frac{-\mathrm{Re}\,[\alpha(z)]}{2Q_\alpha(z)} \\ \mathrm{Im}\,[\beta(z)] &= \frac{-\mathrm{Re}\,[\beta(z)]}{2Q_\beta(z)} \end{aligned} \tag{1}$$

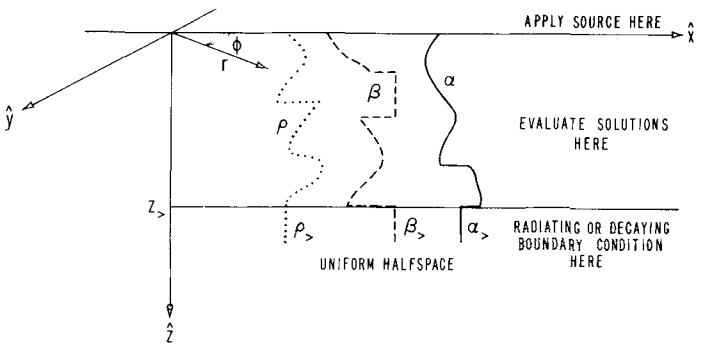

Figure 1. General problem geometry. Seismic velocities and density may be arbitrary piecewise-continuous functions of z between $z = 0$ and $z = z_>$. Beneath $z_>$ a uniform half-space is assumed.

where Q_α and Q_β are the usual attenuative quality factors. This approximation is valid for low loss situations. A trivial modification would allow α and β to be frequency dependent.

Our ultimate objective is to calculate the motions at $z = 0$ which would be generated by a buried point source of seismic waves. We are primarily concerned with seismic sources which can be characterized by a point moment tensor (e.g. explosions and double couples), but results for single forces will be obtained along the way.

2.1 COUPLED DIFFERENTIAL EQUATIONS FOR DISPLACEMENT AND TRACTION

In a vertically inhomogeneous earth, displacement and traction across a horizontal plane are continuous functions of depth regardless of the behaviour of the elastic constants. Numerous authors have exploited this convenient property to obtain sets of coupled ordinary differential equations in z. For example, following Takeuchi & Saito (1972) we expand displacement in a cylindrical coordinate system as

$$\mathbf{u}(r, \phi, z, t) = \frac{1}{2\pi} \int_{-\infty}^{\infty} \exp(-i\omega t) \sum_m \int_0^{\infty} \frac{k}{2\pi} \left[a_1 \mathbf{R}_k^m + a_3 \mathbf{S}_k^m + a_5 \mathbf{T}_k^m \right] dk\, d\omega \tag{2}$$

and traction across a horizontal plane (i.e. the z-component of the stress tensor σ) as

$$\hat{\mathbf{z}} \cdot \sigma(r, \phi, z, t) = \frac{1}{2\pi} \int_{-\infty}^{\infty} \exp(-i\omega t) \sum_m \int_0^{\infty} \frac{k}{2\pi} \left[a_2 \mathbf{R}_k^m + a_4 \mathbf{S}_k^m + a_6 \mathbf{T}_k^m \right] dk\, d\omega \tag{3}$$

where **R**, **S** and **T** are defined in the Appendix, the a_i terms are understood to be functions of k, m, z and ω, and where the sum on m runs from $-\infty$ to ∞. We shall ultimately see that we only need to concern ourselves with $m = -1$, 0 and 1. Our Fourier transform pair is defined in the Appendix, and we allow ω to be complex.

Our objective is to determine the unknown coefficients $a_1, \ldots, a_6$. From the equations of motion, two sets of coupled ordinary differential equations relating $a_1, \ldots, a_6$ can be obtained (Takeuchi & Saito 1972). If we let $\mathbf{a}_P = (a_1, a_2, a_3, a_4)^{\mathrm{T}}$, $\mathbf{a}_H = (a_5, a_6)^{\mathrm{T}}$ and $\mathbf{a}' = d\mathbf{a}/dz$, then the first set of equations, the P–SV equations, is

$$\mathbf{a}_P' = A_P \mathbf{a}_P \tag{4}$$

and the second set, the SH equations, is

$$\mathbf{a}_H' = A_H \mathbf{a}_H \tag{5}$$

where

$$A_P = \begin{bmatrix} 0 & 1/(\rho\alpha^2) & k(1 - 2\beta^2/\alpha^2) & 0 \\ -\omega^2\rho & 0 & 0 & k \\ -k & 0 & 0 & 1/\mu \\ 0 & -k(1 - 2\beta^2/\alpha^2) & [4\mu k^2(1-\beta^2/\alpha^2) - \rho\omega^2] & 0 \end{bmatrix} \tag{6}$$

and

$$A_H = \begin{bmatrix} 0 & 1/\mu \\ \mu k^2 - \rho\omega^2 & 0 \end{bmatrix} \tag{7}$$

with $\mu = \rho\beta^2$. These equations are exact for our cylindrical geometry. Note that m does not appear explicitly in these equations. The continuity of displacement and traction imply that $a_1, \ldots, a_6$ are continuous functions of z. We would like to solve for $a_1, \ldots, a_6$ in the interval $[0, z_>]$, but to do so we must first apply boundary conditions at the ends of the interval.

2.2 RADIATION CONDITION AT $z_>$

Following Kennett & Kerry (1979), let us relate our **a** vector more directly to upgoing and downgoing waves. From this we may derive a radiation condition at $z_>$ by requiring only downgoing waves for $z \geqslant z_>$.

Considering a vector **v** whose elements may be associated with upgoing ($-\hat{z}$ direction) and downgoing wave potentials. For *P–SV*, let

$$\mathbf{v}_P = (\phi_u, \psi_u, \phi_d, \psi_d)^T. \tag{8}$$

and for *SH* let

$$\mathbf{v}_H = (\chi_u, \chi_d)^T. \tag{9}$$

In a uniform medium **v** satisfies

$$\mathbf{v}' = \Lambda\mathbf{v} \tag{10}$$

where for *P–SV*

$$\Lambda_P = \text{diag}\ \{\nu_\alpha, \nu_\beta, -\nu_\alpha, -\nu_\beta\} \tag{11}$$

and for *SH*

$$\Lambda_H = \text{diag}\ \{\nu_\beta, -\nu_\beta\} \tag{12}$$

with

$$\nu_\alpha = \left(k^2 - \frac{\omega^2}{\alpha^2}\right)^{1/2}, \quad \nu_\beta = \left(k^2 - \frac{\omega^2}{\beta^2}\right)^{1/2} \tag{13}$$

and where, in order to ensure that the wavefunction associated with downgoing waves decays with depth, we choose

$$\text{Re}(\nu) \geqslant 0, \quad \text{Im}(\nu) \leqslant 0 \text{ when } \text{Re}(\nu) = 0. \tag{14}$$

If we define vectors

$$\mathbf{b}_P = (a_1, a_3, \omega^{-1}a_2, \omega^{-1}a_4)^T \tag{15}$$

and

$$\mathbf{b}_H = (a_5, \omega^{-1}a_6)^T \tag{16}$$

then our **a** coefficients are related to up- and downgoing waves by

$$\mathbf{v} = D^{-1}\mathbf{b} \tag{17}$$

where for *SH*,

$$D_H^{-1} = \frac{iks_\beta}{\omega}\begin{bmatrix} \beta\nu_\beta & \omega/(\rho\beta) \\ \beta\nu_\beta & -\omega/(\rho\beta) \end{bmatrix} \tag{18}$$

and for *P–SV*

$$D_P^{-1} = \frac{ik}{\rho\omega}\begin{bmatrix} -\omega\eta s_\alpha & \nu_\alpha \delta s_\alpha & -\nu_\alpha s_\alpha & k s_\alpha \\ \nu_\beta \delta s_\beta & -\omega\eta s_\beta & k s_\beta & -\nu_\beta s_\beta \\ \omega\eta s_\alpha & \nu_\alpha \delta s_\alpha & -\nu_\alpha s_\alpha & -k s_\alpha \\ -\nu_\beta \delta s_\beta & \omega\eta s_\beta & -k s_\beta & -\nu_\beta s_\beta \end{bmatrix} \tag{19}$$

with

$$s_\alpha = \omega(2ik\nu_\alpha)^{-1/2}, \quad s_\beta = \omega(2ik\nu_\beta)^{-1/2} \tag{20}$$

$$\eta = \rho\left(\frac{2\mu k^2}{\rho\omega^2} - 1\right), \quad \delta = \frac{2\mu k}{\omega}, \quad \mu = \rho\beta^2.$$

Our physical requirement in the region $z \geqslant z_>$ is that there should be no upgoing waves, i.e. $\phi_u = \psi_u = \chi_u = 0$. Thus, for *P–SV* we must have

$$\phi_u = 0 = [\Omega a_1 + 2\mu k \nu_\alpha a_3 - \nu_\alpha a_2 + k a_4]\,|_{z=z_>^+} \tag{21}$$

$$\psi_u = 0 = [2\mu k \nu_\beta a_1 + \Omega a_3 + k a_2 - \nu_\beta a_4]\,|_{z=z_>^+} \tag{22}$$

where $\Omega = \rho\omega^2 - 2\mu k^2$, and for *SH* we have the boundary condition

$$\chi_u = 0 = [\nu_\beta a_5 + \mu^{-1} a_6]\,|_{z=z_>^+} \tag{23}$$

where

$$z_>^+ = \lim_{\epsilon \to 0} (z_> + |\epsilon|). \tag{24}$$

These boundary conditions are appropriate for all values of ω/k, i.e. for both radiating and evanescent solutions in the half-space $z \geqslant z_>$, except for $|\omega|$ near 0. When $\omega = 0$, (21) and (22) reduce to the same equation. To introduce another independent boundary condition we replace (22) by

$$0 = \left[\frac{1}{\rho\alpha^2} a_2 + 2k\left(1 - \frac{\beta^2}{\alpha^2}\right) a_3 + \frac{1}{\rho\beta^2} a_4\right]\Bigg|_{z=z_>^+}. \tag{25}$$

This follows from replacing the eigenvector matrix D_P by the matrix of generalized eigenvectors. For practical computation, replacement of (22) by (25) is made whenever $|\omega|$ is small, e.g. when $|\omega^2/\beta^2|$ and $|\omega^2/\alpha^2|$ are less than 1 per cent of k^2.

We must stress that this commonly used treatment of the boundary condition at $z_>$ is strictly true only for the case of perfect elasticity (α, β and k real). Borcherdt (1977) has pointed out that a rigorous treatment of anelasticity requires not only α and β but also k to be complex. In addition, because the direction of phase propagation is not generally equal to the direction of mean energy flux in anelastic media, Borcherdt chooses the sign of ν based on the direction of energy transport rather than on the growth or decay of the downgoing vertical wavefunction. Richards (1981) suggests that the choice of a downward decaying wavefunction may be wrong in some cases in anelastic media. Moreover, use of complex ω introduces additional complications, such as causing 'downgoing' waves to propagate upward for small $\mathrm{Re}(\omega)$. Hence, a more rigorous treatment of the boundary condition will probably require the phase of ν_α and ν_β to vary with ω, k, $\alpha_>$ and $\beta_>$.

2.3 BOUNDARY CONDITION AT $z = 0$

Usually in wave propagation problems the Earth's surface is taken to be stress-free, but in this case we choose to apply tractions at the Earth's surface and evaluate the resulting waves at depth. Since source and receiver positions may be ultimately exchanged because of the spatial reciprocity of Green's functions (Aki & Richards 1980, eqn 2.39), this eventually allows us to obtain displacements at the Earth's surface from sources at all possible depths in the interval $[0, z_>]$.

As sources we apply separately tractions at $z = 0$ given by

$$\tilde{\tau}_{\mathrm{L}}^{m} = F_{\mathrm{L}}\, \mathbf{L}_{k}^{m}, \quad \mathbf{L} = \mathbf{R}, \mathbf{S} \text{ or } \mathbf{T}$$

and we further require $F_{\mathrm{L}} = 1$ for all ω, k and m. Then the orthogonality of **R**, **S** and **T** yields the boundary conditions at $z = 0$ given in Table 1 (Takeuchi & Saito 1972, eqns 230 and 240). Note that with this particular choice of F_{L}, nothing in the *P–SV* or *SH* equations or their boundary conditions depends upon m, the azimuthal order. Hence, we do not need to solve the *P–SV* and *SH* equations for individual values of m, even though our ultimate moment tensor source may have a multipolar radiation pattern.

With the specification of this boundary condition, we now have enough information to solve the *P–SV* and *SH* equations for any (ω, k) pair and for the three source terms. Let us denote solutions of the *P–SV* equations for an applied source term $\tilde{\tau}_{\mathrm{L}}$ by $a_{i\mathrm{L}}(z)$, $i = 1, \ldots, 4$, $L = R$ or S, and we denote solutions to the *SH* equations for an applied source $\tilde{\tau}_T$ by $a_{5T}(z)$ and $a_{6T}(z)$. Solutions of the *P–SV* and *SH* equations for more complicated sources such as point moment tensors can be manufactured by taking linear combinations of the ten solutions $a_{1R}, \ldots, a_{6T}$.

2.4 NUMERICAL SOLUTION OF THE BOUNDARY VALUE PROBLEM

Consider the first-order system of differential equations

$$\mathbf{a}' = \mathbf{f}(z, \mathbf{a}), \quad z_0 \leqslant z \leqslant z_> \tag{26}$$

where **a** and **f** are vector functions of order n. For the *P–SV* and *SH* problems, **f** is linear in **a** and can be written as

$$\mathbf{f}(z, \mathbf{a}) = A(z)\,\mathbf{a} + \mathbf{q}(z) \tag{27}$$

where $A(z)$ is an $n \times n$ matrix and $\mathbf{q}(z)$ is a vector of order n. For the *P–SV* problem, $n = 4$, $A = A_P$, and $\mathbf{a} = \mathbf{a}_P$, while for the *SH* problem $n = 2$, $A = A_H$, and $\mathbf{a} = \mathbf{a}_H$.

The system (27) is subject to boundary conditions

$$C_0\,\mathbf{a}(z_0) = \mathbf{c}_0, \quad C_>\,\mathbf{a}(z_>) = \mathbf{c}_> \tag{28}$$

where C_0 is an $n_0 \times n$ matrix and $C_>$ is $(n - n_0) \times n$, $0 \leqslant n_0 \leqslant n$.

For the *P–SV* problem, from Table 1 we see that

$$C_0 = \begin{bmatrix} 0 & 1 & 0 & 0 \\ 0 & 0 & 0 & 1 \end{bmatrix} \tag{29}$$

and for a $\tilde{\tau}_R$ source, $\mathbf{c}_R = (-F_R, 0)^{\mathrm{T}}$, while for a $\tilde{\tau}_S$ source $\mathbf{c}_S = (0, -F_S)^{\mathrm{T}}$. At the top of the uniform half-space, the *P–SV* boundary condition obtained from (21) and (22) is given by $\mathbf{c}_> = (0, 0)^{\mathrm{T}}$ with

$$C_> = \begin{bmatrix} \Omega & -\nu_\alpha & 2\mu k \nu_\alpha & k \\ 2\mu k \nu_\beta & k & \Omega & -\nu_\beta \end{bmatrix}\Bigg|_{z = z_>^+} \tag{30}$$

Table 1. Boundary condition at $z = 0$ for various sources.

Source term	a_2	a_4	a_6
$\tilde{\tau}_R$	-1	0	★
$\tilde{\tau}_S$	0	-1	★
$\tilde{\tau}_T$	★	●	-1

★Not applicable due to separation of *P–SV* and *SH*.

for $|\omega|$ not near 0, and for $|\omega|$ near 0 (see Section 2.3)

$$C_> = \begin{bmatrix} \Omega & -\nu_\alpha & 2\mu k \nu_\alpha & k \\ 0 & 1/(\rho\alpha^2) & 2k(1-\beta^2/\alpha^2) & \mu^{-1} \end{bmatrix}\Bigg|_{z=z_>^+}. \tag{31}$$

For the *SH* problem, from Table 1 we obtain $C_0 = (0 \;\; 1)$, $\mathbf{c}_0 = -F_T$, $C_> = (\nu_\beta \;\; \mu^{-1})$, and $\mathbf{c}_> = 0$.

An approximate solution $\mathbf{a}^h(z)$ is sought for $\mathbf{a}(z)$ on a mesh

$$z_0 = z_1 < z_2 < \ldots < z_{N+1} = z_> \tag{32}$$

$$h_i = z_{i+1} - z_i, \quad h = \max_{1 \leqslant i \leqslant N} h_i.$$

In the collocation method, given l points ($l \geqslant 1$)

$$0 \leqslant \xi_1 < \xi_2 < \ldots < \xi_l \leqslant 1$$

the approximation $\mathbf{a}^h(z)$ is required to be a continuous piecewise polynomial vector function satisfying:

(C1) On each element of the mesh (z_i, z_{i+1}), each component of $\mathbf{a}^h$ is a polynomial of degree at most l.

(C2) $\mathbf{a}^h(z)$ is continuous throughout $[z_0, z_>]$

(C3) $\mathbf{a}^h(z)$ satisfies the differential equation (26) exactly at the collocation points

$$z_{ij} = z_i + h_i \xi_j, \quad 1 \leqslant j \leqslant l, \quad 1 \leqslant i \leqslant N. \tag{33}$$

(C4) $\mathbf{a}^h(z)$ satisfies the boundary conditions (28).

Thus, as in the usual finite element method, the collocation solution is a piecewise polynomial function; however, no variational principle is used here and the differential equations (26) are approximated directly by the requirement (C3). Also, like other finite element methods, the collocation method presented here is equivalent to certain non-trivial, high-order finite difference schemes as outlined below.

If the problem is sufficiently smooth and an isolated solution $\mathbf{a}(z)$ exists, Weiss (1974) has shown that by choosing $\xi_1, \ldots, \xi_l$ as the Gaussian points (zeros of the Legendre polynomial of degree l on $[0, 1]$), we get

$$\max_{1 \leqslant j \leqslant n} [a_j(z_i) - a_j^h(z_i)] = O(h^{2l}), \qquad 1 \leqslant i \leqslant N+1, \tag{34}$$

i.e. the maximum discrepancy is $O(h^{2l})$.

If the function $\mathbf{f}(z, \mathbf{a})$ in (26) or $A(z)$ in (27) has, at worst, jump discontinuities at some points

$$z_0 \leqslant w_1 < \ldots < w_M \leqslant z_>$$

[as would be the case if $\alpha(z)$, $\beta(z)$ or $\rho(z)$ had discontinuities at those depths], then these points w_i must be included in the mesh (32). In this case the error estimate (34) still holds because even if $\mathbf{f}$ were to have a jump discontinuity at $z = z_j$, $\mathbf{a}(z)$ would still be continuous at z_j (with discontinuous higher derivatives). This behaviour could be duplicated by $\mathbf{a}^h(z)$, which is also merely continuous at mesh points. Moreover, $\mathbf{f}[z, \mathbf{a}^h(z)]$ is only evaluated at the collocation points z_{ij} (33), and if we require $\xi_1 > 0$, $\xi_l < 1$, which is true for Gaussian points, then the collocation points are never mesh points and $\mathbf{f}[z_{ij}, \mathbf{a}^h(z_{ij})]$ is always single valued.

For implementation purposes, note that the above collocation scheme is equivalent to an implicit Runge-Kutta method, since $\mathbf{a}^h(z_{i+1})$ may be obtained by using Gaussian quadrature to integrate the differential equation on the interval $[z_i, z_{i+1}]$. Let

$$\mathbf{a}_i = \mathbf{a}^h(z_i), \quad \mathbf{f}_{ij} = \mathbf{f}[z_{ij}, \mathbf{a}^h(z_{ij})] = [\mathbf{a}^h(z_{ij})]', \quad 1 \leqslant j \leqslant l. \tag{35}$$

By using Gaussian quadrature we obtain the difference scheme

$$\mathbf{a}_{i+1} = \mathbf{a}_i + h_i \sum_{j=1}^{l} \lambda_j \mathbf{f}_{ij} \tag{36}$$

$$\mathbf{f}_{ij} = \mathbf{f}\left(z_{ij}, \quad \mathbf{a}_i + h_i \sum_{q=1}^{l} \zeta_{jq} \mathbf{f}_{iq}\right), \quad 1 \leqslant j \leqslant l \tag{37}$$

where λ_j and ζ_{jq} are quadrature constants given by

$$\zeta_{jq} = \int_0^{\xi_j} L_q(t)\, dt, \quad \lambda_j = \int_0^1 L_j(t)\, dt, \quad 1 \leqslant j, q \leqslant l \tag{38}$$

and L_j are the Lagrange polynomials

$$L_j(t) = \prod_{\substack{q=1 \\ q \neq j}}^{l} (t - \xi_q) \Bigg/ \prod_{\substack{q=1 \\ q \neq j}}^{l} (\xi_j - \xi_q)$$

as in Weiss (1974).

From (36) and (37) it can be seen that $\mathbf{f}_{ij}$ can be eliminated locally for each i, $1 \leqslant i \leqslant N$. We describe this process for the linear case (27). A quasi-linearization process may be used for a general non-linear problem (Keller 1976). Defining the vectors of order nl,

$$\mathbf{f}_i = \begin{bmatrix} \mathbf{f}_{i1} \\ \cdot \\ \cdot \\ \cdot \\ \mathbf{f}_{il} \end{bmatrix}, \quad \mathbf{r}_i = \begin{bmatrix} \mathbf{q}(z_{i1}) + A(z_{i1})\mathbf{a}_i \\ \cdot \\ \cdot \\ \cdot \\ \mathbf{q}(z_{il}) + A(z_{il})\mathbf{a}_i \end{bmatrix} \tag{39}$$

(37) may be written

$$J_i \mathbf{f}_i = \mathbf{r}_i \tag{40}$$

where J_i is the $nl \times nl$ matrix

$$J_i = I - h_i \begin{bmatrix} \zeta_{11} A(z_{i1}) & \zeta_{12} A(z_{i1}) & \cdots & \zeta_{1l} A(z_{i1}) \\ \zeta_{21} A(z_{i2}) & \zeta_{22} A(z_{i2}) & \cdots & \zeta_{2l} A(z_{i2}) \\ \cdot & & & \cdot \\ \cdot & & & \cdot \\ \cdot & & & \cdot \\ \cdot & & & \cdot \\ \zeta_{l1} A(z_{il}) & \cdots & & \zeta_{ll} A(z_{il}) \end{bmatrix} \tag{41}$$

and where I is the $nl \times nl$ identity matrix. So, (36) gives

$$\mathbf{a}_{i+1} = \mathbf{a}_i + h_i \boldsymbol{\lambda}^{\mathrm{T}} \mathbf{f}_i = \mathbf{a}_i + h_i \boldsymbol{\lambda}^{\mathrm{T}} J_i^{-1} \mathbf{r}_i. \tag{42}$$

Writing $J_i^{-1} = [(J_i^{-1})_{jq}]$ with each $(J_i^{-1})_{jq}$ an $n \times n$ block, we get the finite difference scheme

$$\mathbf{a}_{i+1} = \Gamma_i \mathbf{a}_i + \mathbf{g}_i, \quad i = 1, \ldots, N \tag{43}$$

$$C_0 \mathbf{a}_1 = \mathbf{c}_0, \quad C_> \mathbf{a}_{N+1} = \mathbf{c}_>, \tag{44}$$

where Γ_i is an $n \times n$ matrix and $\mathbf{g}_i$ an n-vector,

$$\Gamma_i = I + h_i \sum_{j=1}^{l} \lambda_j \sum_{q=1}^{l} (J_i^{-1})_{jq} A(z_{iq}), \quad 1 \leqslant i \leqslant N \tag{45}$$

$$\mathbf{g}_i = h_i \sum_{j=1}^{l} \lambda_j \sum_{q=1}^{l} (J_i^{-1})_{jq} \mathbf{q}(z_{iq}).$$

Note that Γ_i is the collocation approximation of the propagator matrix.

In generating Γ_i and $\mathbf{g}_i$ for each element i, the matrix J_i is factored rather than explicitly inverted and the linear systems of order nl are solved for $n+1$ right-hand side vectors. In our particular problem $\mathbf{g} = \mathbf{q} = 0$ since the source is introduced as a boundary value.

The system of linear equations (43) and (44) to be solved is written as

$$\begin{bmatrix} C_0 & & & & \\ -\Gamma_1 & I & & 0 & \\ & -\Gamma_2 & I & & \\ & & \ddots & \ddots & \\ & 0 & & -\Gamma_N & I \\ & & & & C_> \end{bmatrix} \begin{bmatrix} \mathbf{a}_1 \\ \mathbf{a}_2 \\ \cdot \\ \cdot \\ \mathbf{a}_N \\ \mathbf{a}_{N+1} \end{bmatrix} = \begin{bmatrix} \mathbf{c}_0 \\ \mathbf{g}_1 \\ \mathbf{g}_2 \\ \cdot \\ \cdot \\ \mathbf{g}_N \\ \mathbf{c}_> \end{bmatrix} \tag{46}$$

and is solved by the package SOLVEBLOK (de Boor & Weiss 1980), which exploits the sparseness of the large matrix by performing Gauss elimination with scaled row partial pivoting on the non-zero subpartitions of the matrix. For the *P–SV* problem, note that the matrix of (46) is the same for τ_R and τ_S sources. Thus, it needs to be assembled and factored only once. Consequently, the computational cost of obtaining the two corresponding solutions is essentially that of obtaining only one.

The collocation method (36)–(37) which we use is particularly competitive when the

eigenvalues of $A(z)$ have large positive and negative real parts. This corresponds to the case of highly evanescent solutions of the *P–SV* and *SH* problems. Let $\lambda_1, \ldots, \lambda_n$ be the eigenvalues of $A(z)$. The real parts of these eigenvalues are assumed to stay away from 0 over the interval of integration and we denote

$$\lambda_- = \min_{j,\,z} \mathrm{Re}(\lambda_j) < 0, \quad \lambda_+ = \max_{j,\,z} \mathrm{Re}(\lambda_j) > 0. \tag{47}$$

It is well known that methods which employ initial value integrations (or propagator matrices) run into trouble when λ_+ and λ_- are large, because they have to integrate rapidly (exponentially) increasing fundamental solution components, producing exponentially increasing roundoff errors. However, when the fundamental solution components are finally combined to form the solution of the boundary value problem, the growing fundamental solution components are scaled down by the boundary conditions (assuming that the boundary value problem is well-posed) and their contribution to the actual solution of the problem (26), (28), is negligible away from the boundaries z_0 and $z_>$.

The method presented here remains stable even under these circumstances. To see why, recall that a difference scheme of the form (43) is said to be A-stable if, when applied to the test equation $a' = \lambda a$, $z \geqslant z_0$, with λ a constant satisfying $\mathrm{Re}(\lambda) < 0$, the condition $|a_{i+1}| \leqslant |a_i|$ is satisfied for any $h_i > 0$. Our collocation method has the property of A-stability in both directions of integration, in z and in $-z$. Thus, the numerical solution to the homogeneous problem does not grow in magnitude. As a result, stable accurate solutions are obtained for arbitrarily large λ_+ and λ_-, provided that an appropriate mesh (32) is used. Such a mesh is dense where the actual solution, not the propagator matrix, varies quickly, and is sparse elsewhere. Despite the possibly extreme non-uniformity of the resulting mesh, the linear system (46) can be safely solved because the condition number of the matrix, which roughly indicates the factor by which roundoff errors are amplified when solving (46), is only $O(N)$ and is independent of

$$\left(\min_{1 \leqslant i \leqslant N} h_i \right)^{-1}$$

The use of SOLVEBLOK for this purpose is preferred over the factorization method in which (43) is used in a direct recursion to express $\mathbf{a}_{N+1}$ in terms of $\mathbf{a}_1$ and obtain from (44) an $n \times n$ linear system for $\mathbf{a}_1$.

The complete theory for collocation for this type of problem was given by Ascher & Weiss (1982a, b). It includes more precise statements along the lines above and their proofs, as well as formulae for selecting the mesh (32) to achieve a specified accuracy. The basic idea when selecting a mesh is to try to equidistribute the error, i.e. to have roughly the same error magnitude at each mesh point. In general, such a mesh can only be chosen after some quantitative knowledge of the solution profile is available. However, near z_0 the solution of the boundary value problem is dominated by the component $\exp[\lambda_-(z-z_0)]$ and so an *a priori* mesh selection can be made there. For the *SH* and *P–SV* problems the mesh can be taken very sparse elsewhere. The total number of mesh points N (but not their location near z_0) is essentially independent of the eigenvalues of $A(z)$, provided that their real parts are large enough in magnitude. As the number of collocation points l increases, the number of mesh points required to approximate $\exp[\lambda_-(z-z_0)]$ to a desired accuracy decreases. Of course, the computational effort per mesh point increases with l, and we have found $l = 3$ or 4 most economical.

For rapidly oscillatory solutions the collocation method is less well suited, although it still works. For these solutions the mesh must be dense everywhere and the collocation method is not particularly more efficient or stable than initial value techniques.

2.5 DISPLACEMENTS AND STRAINS FROM POINT FORCES

Having obtained $a_{1R}(z), \ldots, a_{6T}(z)$ for any choice of ω and k, following Olson *et al.* (1983) we wish to find the particular linear combinations of these solutions which will give us displacements and strains from a point force.

Let $\tilde{\mathbf{u}}_L^m$ be the transformed displacements caused by a $\tilde{\boldsymbol{\tau}}_L^m$ source, where $L = R$, S or T. From (2) and (A9) we obtain

$$\tilde{\mathbf{u}}_L^m = a_{1L}\,\mathbf{R}_k^m + a_{3L}\,\mathbf{S}_k^m + a_{5L}\,\mathbf{T}_k^m \tag{48}$$

where $a_{5R} = a_{5S} = a_{1T} = a_{3T} = 0$ due to the separation of P–SV and SH. The transformed displacements $\tilde{\mathbf{u}}^n$ caused by a point force in the $\hat{\mathbf{x}}_n$-direction, where $n = 1$, 2 or 3, are

$$\tilde{\mathbf{u}}^n = \sum_m \left(f_R^n\,\tilde{\mathbf{u}}_R^m + f_S^n\tilde{\mathbf{u}}_S^m + f_T^n\,\tilde{\mathbf{u}}_T^m\right) \tag{49}$$

where the f^n terms are expansion coefficients for a point force applied at r_0, ϕ_0 in the $\hat{\mathbf{x}}_n$-direction given by

$$\mathbf{f} = F_0\,\frac{\delta(r-r_0)}{r_0}\,\delta(\phi-\phi_0)\,\delta(z)\,\delta(t)\,\hat{\mathbf{x}}_n, \qquad n = 1, 2, 3. \tag{50}$$

The Fourier transform of the resulting traction per unit impulse is

$$\bar{\boldsymbol{\tau}}^n = \frac{\delta(r-r_0)}{r_0}\,\delta(\phi-\phi_0)\,\hat{\mathbf{x}}_n \tag{51}$$

which may be expanded as

$$\bar{\boldsymbol{\tau}}^n = \sum_m \int_0^\infty \frac{k}{2\pi}\left(f_R^n\,\mathbf{R}_k^m + f_S^n\mathbf{S}_k^m + f_T^n\mathbf{T}_k^m\right) dk. \tag{52}$$

From (A4) and (A5) we obtain

$$f_L^n = \int_0^{2\pi}\int_0^\infty r\,\bar{\boldsymbol{\tau}}^n \cdot \mathbf{L}_k^{m*}\,dr\,d\phi, \qquad n = 1, 2, 3, \quad \mathbf{L} = \mathbf{R}, \mathbf{S}, \mathbf{T}. \tag{53}$$

In the limit as $r_0 \to 0$, $\phi_0 \to 0$, (53) yields the point force expansion coefficients required in (49) and given in Table 2. Although the sum on m in (49) nominally runs from $-\infty$ to ∞, only the $m = -1$, 0 and 1 terms contribute because of the m dependence of the point force expansion coefficients. By performing the sum on m, and by using (48), (49), Table 2, and (A1) we obtain the displacement Green's functions

$$\begin{aligned}\tilde{\mathbf{u}}^1 = {} & \hat{\mathbf{z}}\cos\phi\,[a_{1S}J_1] \\ & + \hat{\mathbf{r}}\cos\phi\left[\left(J_0 - \frac{1}{kr}J_1\right)a_{3S} + \frac{1}{kr}J_1 a_{5T}\right] \\ & - \hat{\boldsymbol{\phi}}\sin\phi\left[\frac{1}{kr}J_1 a_{3S} + \left(J_0 - \frac{1}{kr}J_1\right)a_{5T}\right]\end{aligned} \tag{54a}$$

$$\begin{aligned}\tilde{\mathbf{u}}^2 = {} & \hat{\mathbf{z}}\sin\phi\,[a_{1S}J_1] \\ & + \hat{\mathbf{r}}\sin\phi\left[\left(J_0 - \frac{1}{kr}J_1\right)a_{3S} + \frac{1}{kr}J_1 a_{5T}\right] \\ & + \hat{\boldsymbol{\phi}}\cos\phi\left[\frac{1}{kr}J_1 a_{3S} + \left(J_0 - \frac{1}{kr}J_1\right)a_{5T}\right]\end{aligned} \tag{54b}$$

$$\tilde{\mathbf{u}}^3 = \hat{\mathbf{z}}a_{1R}J_0 - \hat{\mathbf{r}}a_{3R}J_1, \tag{54c}$$

Table 2. Point force expansion coefficients.

n	f_R^n	f_S^n	f_T^n
1	0	$m\Delta_{m1}$	$-i\Delta_{m1}$
2	0	$-i\Delta_{m1}$	$-m\Delta_{m1}$
3	δ_{m0}	0	0

$\Delta_{mn} = \frac{1}{2}(\delta_{mn} + \delta_{-mn})$.

where the Bessel functions J_0 and J_1 implicitly have the argument (kr). If we define the strain tensor elements resulting from a point force in the $\hat{\mathbf{x}}_n$-direction to be

$$e_{ij}^n = \tfrac{1}{2}\left(\frac{\partial}{\partial x_i} u_j^n + \frac{\partial}{\partial x_j} u_i^n\right), \tag{55}$$

they may be evaluated at $\phi = 0$ in Fig. 2. They are, for an $\hat{\mathbf{x}}_1$ point force,

$$\begin{aligned}
\tilde{e}^{\,1}_{11} &= X_1(a_{5T} - a_{3S}) - kJ_1 a_{3S} \\
\tilde{e}^{\,1}_{13} &= \tfrac{1}{2}X_2(ka_{1S} + a'_{3S}) + \frac{J_1}{2kr} a'_{5T} \\
\tilde{e}^{\,1}_{22} &= (a_{3S} - a_{5T}) X_1 \\
\tilde{e}^{\,1}_{33} &= a'_{1S} J_1 \\
\tilde{e}^{\,1}_{12} &= \tilde{e}^{\,1}_{23} = 0,
\end{aligned} \tag{56}$$

for an $\hat{\mathbf{x}}_2$ point force,

$$\begin{aligned}
\tilde{e}^{\,2}_{12} &= -X_1(a_{5T} - a_{3S}) - \tfrac{1}{2}kJ_1 a_{5T} \\
\tilde{e}^{\,2}_{23} &= \tfrac{1}{2}\left(a_{1S}\frac{J_1}{r} + a'_{3S}\frac{J_1}{kr} + a'_{5T}X_2\right) \\
\tilde{e}^{\,2}_{11} &= \tilde{e}^{\,2}_{22} = \tilde{e}^{\,2}_{33} = \tilde{e}^{\,2}_{13} = 0,
\end{aligned} \tag{57}$$

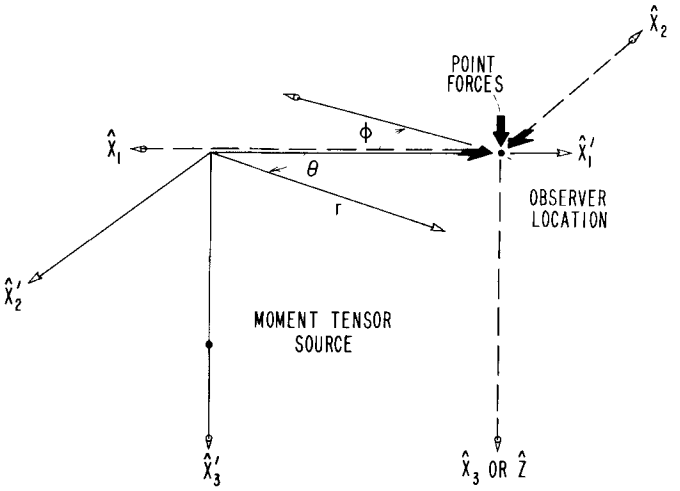

Figure 2. Representation theorem geometry. Moment tensor sources are simulated by applying point forces at the observer locations and calculating the resulting strains at the moment tensor source location. The strain tensor is calculated in the unprimed coordinate system and rotated into the primed coordinate system.

and for an $\hat{\mathbf{x}}_3$ point force,

$$\tilde{e}^{\,3}_{11} = -a_{3R}\, kX_2$$
$$\tilde{e}^{\,3}_{13} = -\tfrac{1}{2} J_1(a_{1R} k + a'_{3R}) \tag{58}$$
$$\tilde{e}^{\,3}_{22} = -a_{3R}\, \frac{J_1}{r}$$
$$\tilde{e}^{\,3}_{33} = a'_{1R}\, J_0,$$

where J_0 and J_1 are Bessel functions with argument (kr), and where

$$a' = \frac{da}{dz}$$
$$X_1 = \frac{J_0}{r} - \frac{2}{kr^2} J_1$$
$$X_2 = J_0 - \frac{J_1}{kr}.$$

In practice the a'_1, a'_3 and a'_5 terms may be obtained from a_2, a_4 and a_6 by using the *P–SV* and *SH* differential equations, (4) and (5). Note that while $a_1, \ldots, a_6$ are continuous across discontinuities in material properties, their derivatives are not. Consequently, some care must be taken when evaluating a'_1, a'_3 and a'_5 at the depths of material discontinuities.

2.6 INTRODUCING A MOMENT TENSOR SOURCE

To include the effect of a moment tensor source we use the approach of Olson *et al.* (1983), which we briefly summarize here.

The spectrum of the n component of displacement at the observer location, $\mathbf{y} = (r, \vartheta = 0, z = 0)$ in Fig. 2, is given by

$$\bar{u}_n(\mathbf{y}) = \bar{m}_{kl}(\mathbf{x})\, \bar{\epsilon}^n_{kl}(\mathbf{x}, \omega; \mathbf{y}, 0) \tag{59}$$

where m_{kl} are the elements of the moment tensor of a point source located at $\mathbf{x} = (r = 0, \vartheta = 0, x'_3)$, ϵ^n_{kl} are the elements of the strain tensor evaluated at $\mathbf{x}$ caused by application of an impulsive point force at $\mathbf{y}$ and time 0 in the $\hat{\mathbf{x}}'_n$ direction, as illustrated in Fig. 2, and where the summation convention over repeated indices is used. Note that m_{kl} and ϵ_{kl} are components with respect to the $\hat{\mathbf{x}}'_1$–$\hat{\mathbf{x}}'_2$–$\hat{\mathbf{x}}'_3$ basis system, whereas e_{kl} (55) are components in the $\hat{\mathbf{x}}_1$–$\hat{\mathbf{x}}_2$–$\hat{\mathbf{x}}_3$ basis. The two strain tensors are related by

$$\epsilon^n = \begin{bmatrix} -e^n_{11} & -e^n_{12} & e^n_{13} \\ -e^n_{21} & -e^n_{22} & e^n_{23} \\ e^n_{31} & e^n_{32} & -e^n_{33} \end{bmatrix}, \quad n = 1 \text{ or } 2 \tag{60a}$$

and

$$\epsilon^3 = \begin{bmatrix} e^3_{11} & e^3_{12} & -e^3_{13} \\ e^3_{21} & e^3_{22} & -e^3_{23} \\ -e^3_{31} & -e^3_{32} & e^3_{33} \end{bmatrix}, \tag{60b}$$

which is obtained by rotating the elements of e by π and changing the sign of e for $n = 1$ and 2. To obtain displacements at $\vartheta \neq 0$, rather than move the observation location we instead rotate the seismic source by an angle of $-\vartheta$, which is physically equivalent to moving the observer. This rotation changes the moment tensor elements m_{pq} to m'_{pq} where

$$
\begin{aligned}
m'_{11} &= m_{11}\cos^2\vartheta + m_{12}\sin 2\vartheta + m_{22}\sin^2\vartheta \\
m'_{12} &= m_{12}\cos 2\vartheta + \tfrac{1}{2}(m_{22} - m_{11})\sin 2\vartheta \\
m'_{13} &= m_{13}\cos\vartheta + m_{23}\sin\vartheta \\
m'_{22} &= m_{11}\sin^2\vartheta - m_{12}\sin 2\vartheta + m_{22}\cos^2\vartheta \\
m'_{23} &= -m_{13}\sin\vartheta + m_{23}\cos\vartheta \\
m'_{33} &= m_{33},
\end{aligned}
\tag{61}
$$

and $m'_{ij} = m'_{ji}$. Thus, the representation theorem becomes

$$
\begin{aligned}
\bar{u}_r(r, \vartheta) &= \bar{m}'_{kl}\,\bar{\epsilon}^1_{kl} \\
\bar{u}_\vartheta(r, \vartheta) &= \bar{m}'_{kl}\,\bar{\epsilon}^2_{kl} \\
\bar{u}_z(r, \vartheta) &= \bar{m}'_{kl}\,\bar{\epsilon}^3_{kl}
\end{aligned}
\tag{62}
$$

where u_r, u_ϑ and u_z are the radial outward, azimuthal and vertical downward components of motion in the $\hat{\mathbf{x}}'_1$–$\hat{\mathbf{x}}'_2$–$\hat{\mathbf{x}}'_3$ coordinate system, m' is the rotated moment tensor given by (61) and ϵ^n is the strain tensor caused by a point force in the $\hat{\mathbf{x}}'_n$-direction at $(r, 0)$, given by (60).

3 An example

We illustrate the various steps in the CSM by calculating complete theoerical seismograms in a velocity structure consisting of a linear velocity-gradient region overlying a uniform half-space. This model is shown in Fig. 3 and its parameters are given in Table 3. The model has been chosen to be perfectly elastic in order to enable direct comparison with DWFE results.

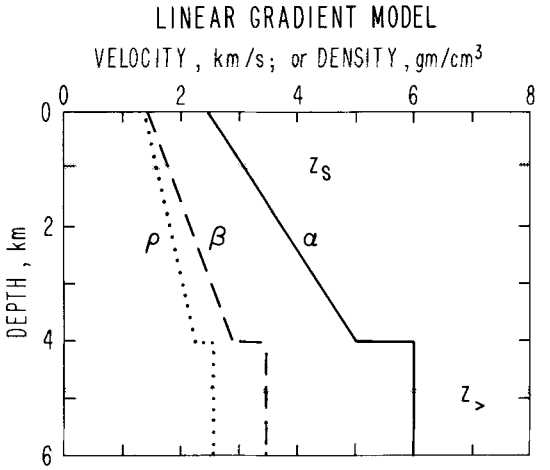

Figure 3. Linear gradient test example. The radiation condition is applied at depth $z_>$ and solutions obtained at z_s and $z_>$ are shown in subsequent figures.

Table 3. Linear gradient model.

Depth, km	α, km s^{-1}	β, km s^{-1}	ρ, g cm^{-3}	Q_α	Q_β
0	2.50	1.44	1.39	∞	∞
4	5.00	2.89	2.28	∞	∞
4	6.00	3.46	2.58	∞	∞
$\geqslant$4.924	6.00	3.46	2.58	∞	∞

The first step is the choice of a suitable grid of points in the ω–k plane at which to obtain solutions of the *P–SV* and *SH* equations. In our test case we obtain solutions at points (ω_n, k_m) given by

$$\omega_n = \frac{1}{T}(2\pi n - i \ln D), \quad n = 0, 1, \ldots, \qquad 0 \leqslant \mathrm{Re}(\omega) \leqslant 2\pi$$

$$J_1(k_m R) = 0, \quad 0 \leqslant k_m \leqslant 8.56$$

where $T = 32.768$ s is the length of the desired time series, $D = 0.05$ is the exponential decay factor at the end of the time series (see Appendix), and $R = 110$ km is the reflecting cylinder radius (see Appendix). This portion of the ω–k plane is more than adequate to include the complete response of the medium in the 0–1 Hz band.

The collocation method is then used to obtain solutions $a_{1R}(z), \ldots, a_{6T}(z)$ at each ω–k point. Representative solutions for a_{1R} and a_{5T} are shown in Figs 4 and 5. In each figure, ω is held fixed at the value shown and k is chosen to give horizontal phase velocities ω/k of 0.5, 1.5, 2.5 and 3.5 km s^{-1}. The values of the solutions at the mesh points (+ symbols) are determined by the collocation method, and the smooth curves connecting them are their Hermite cubic interpolants.

The solutions depicted in Figs 4 and 5 show the intuitively expected behaviour. Below the geometric optics *S*-wave turning point (indicated by arrows), the solutions decay exponentially while above the turning point they are oscillatory. For the 0.5 km s^{-1} phase

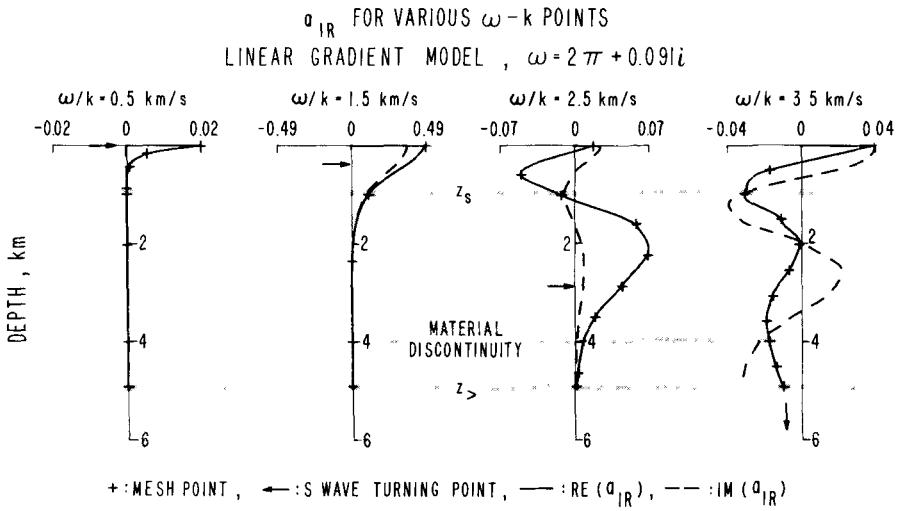

Figure 4. Real and imaginary parts of solution a_{1R} for a fixed ω and varying phase velocity, ω/k. Arrows indicate depth of *S*-wave turning point for each phase velocity. Crosses are solution points obtained by collocation method, and the smooth connecting curves are interpolating functions. Solutions from depths z_S and $z_>$ are shown in subsequent figures.

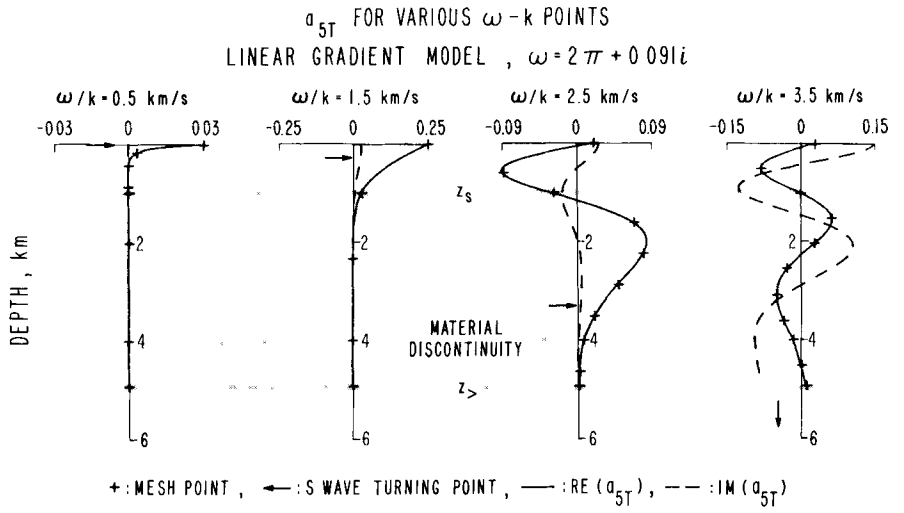

Figure 5. Real and imaginary parts of solution a_{sT} for a fixed ω and varying phase velocity ω/k. See Fig. 4 for details.

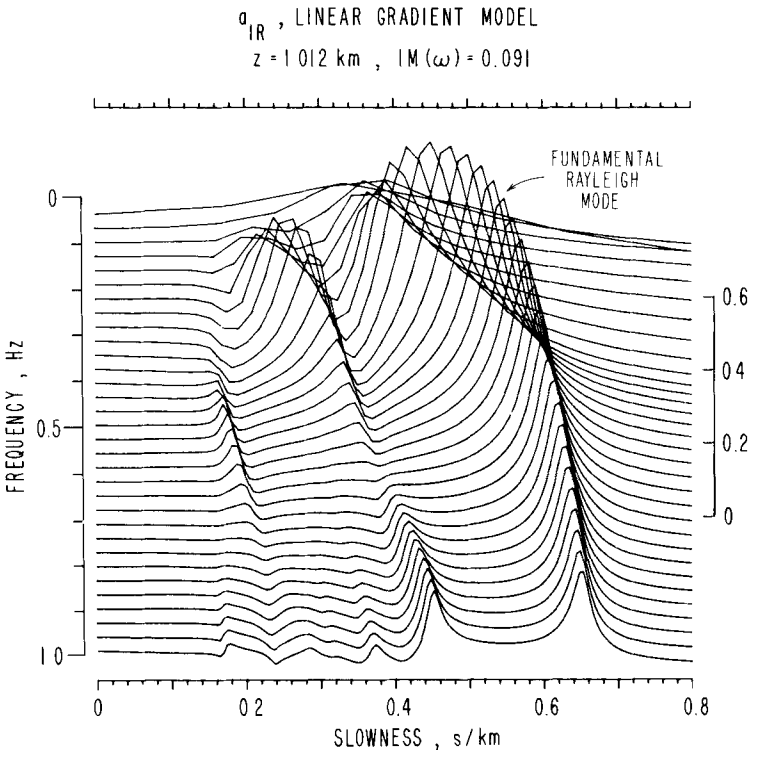

Figure 6. Solution for a_{1R} at $z_s = 1.012$ km depth in the linear gradient model of Fig. 3. Solution is shown as a function of frequency, $\omega/2\pi$, and slowness, k/ω. All traces are plotted in record section format to the common scale shown on the right, and any static offset has been removed from all traces.

velocity, which is less than β at the surface, S-waves do not penetrate into the medium at all and the solutions decay rapidly away from the surface. For 1.5 and 2.5 km s^{-1} phase velocities the S-waves turn within the linear gradient zone but are still evanescent in the underlying half-space. Finally, for a 3.5 km s^{-1} phase velocity S-waves can radiate out into the underlying uniform half-space. The boundary condition at $z_>$ changes from a decaying to a radiating condition, and solutions in the interval $[0, z_>]$ are completely oscillatory. Note that the solutions are continuous across the material discontinuity at 4 km depth, as they should be.

These solutions may also be viewed as functions of ω and k for particular depths. In Figs 6 and 7 a_{1R} is shown as a function of ω and horizontal slowness, k/ω, for the two depths indicated in the previous figures, $z_s = 1.012$ km and $z_> = 4.924$ km. At the shallower depth, the dominant feature is the ridge caused by the fundamental Rayleigh mode. For low frequencies this mode has a phase velocity or slowness appropriate to the region $z > z_>$, but as the frequency increases the phase velocity of the mode diminishes. For the deeper depth (Fig. 7) the fundamental mode is still apparent at low frequencies but it disappears as the frequency increases.

Since these solutions are obtained for a predetermined portion of the ω–k plane, one can easily exclude portions of the earth model's seismic response simply by not calculating solutions for that portion of the ω–k plane. This is similar to the phase velocity windowing employed in the reflectivity method of Fuchs & Müller (1971) and others' subsequent work, and it simultaneously economizes the calculation and makes the resulting seismograms more easily interpretable.

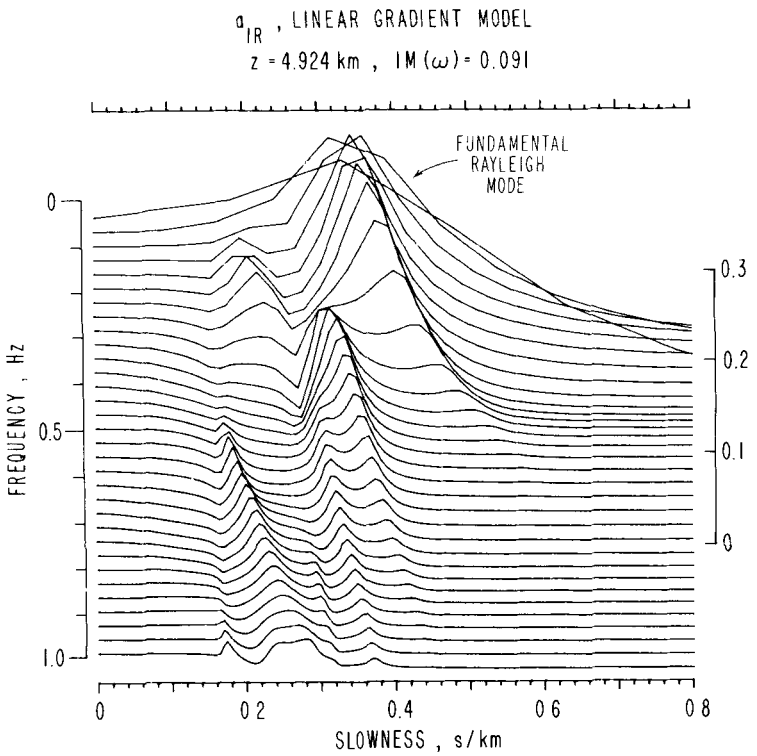

Figure 7. Solution for a_{1R} at $z_> = 4.924$ km depth in the linear gradient model. See Fig. 6 for details.

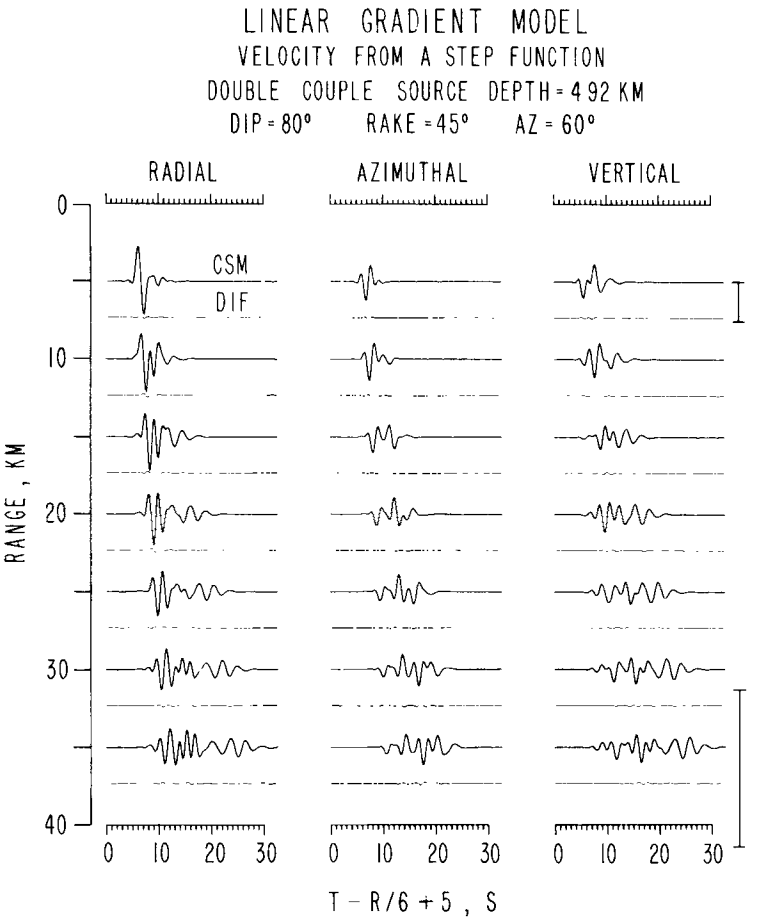

Figure 8. Theoretical velocity seismograms for a point dislocation having equal thrust and left-lateral components on a dipping plane in the linear gradient model of Fig. 1. Source depth is 4.924 km, moment is 10^{20} dyne cm, and source time function is a step function. Seismograms have been plotted with a reduction velocity of 6 km s^{-1}, and have been filtered with a zero-phase cosine-squared taper between 0.5 and 1 Hz. For each range and component two traces are shown. The upper, heavier trace is the collocation seismogram and the lower, lighter trace is the difference between it and the equivalent DWFE seismogram. The amplitude scale varies linearly with range. The vertical bars to the right of the vertical seismograms indicate 0.001 cm s^{-1} at 5 and 35 km range respectively.

Once the solutions $a_{1R}, \ldots, a_{6T}$ are available on the desired region of the ω–k plane, theoretical seismograms are obtained by calculating the strain tensor, doing the inverse transforms, and contracting the strain tensor with a source moment tensor. As an example, the heavier lines in Fig. 8 are collocation seismograms calculated for a point double couple of moment 10^{20} dyne cm located at depth $z_> = 4.924$ km in the linear gradient model. The source has a dip of 80°, a rake of 45°, and is observed at an azimuth $\vartheta = 60°$ (Fig. 2) off strike. The source time dependence is a step function and the seismograms are ground velocity in the frequency band 0–1 Hz. The seismograms have been filtered by application of a cosine-squared fading of their spectra between 0.5 and 1 Hz.

In order to check the CSM, we have also calculated seismograms for the identical test problem using the DWFE method. Rather than show the DWFE seismograms directly, in Fig. 8 we have plotted the difference between the CSM and DWFE seismograms using the

lighter lines. As can be seen, the methods agree rather well for this problem. In general the discrepancies between the methods appear to be due to slight differences in phase rather than waveform mismatches, and it is not yet clear which set of seismograms is more accurate.

Although omitted here for brevity's sake, we have performed other tests of the CSM with satisfactory results. Analytic solutions to (4) and (5) and their boundary conditions can easily be found for the case of a uniform layer overlying a uniform half-space, and in all cases for which the analytic solution can be evaluated accurately, the collocation method obtains the proper solution within the desired tolerance. In addition, we have successfully duplicated the theoretical seismograms obtained by Olson *et al.* (1983) for an earth model consisting of two uniform layers overlying a uniform half-space.

4 Discussion

In this paper we have demonstrated the utility of collocation techniques in solving boundary value problems for stress-displacement vectors in a vertically varying medium. While the collocation solver has been placed into a flexible, general purpose package for the calculation of synthetic seismograms, we have not yet attempted to optimize the efficiency of the package.

The computation time required by the current version of the CSM is roughly proportional to the cube of the desired frequency bandwidth (see Appendix for details). The efficiency of the CSM is largely dependent upon two factors, the number of sample points required in the ω–k plane for accurate evaluation of the integral transforms, and the rapidity with which individual solutions are obtained, especially for large $\mathrm{Re}(\omega)$. Improvements in both of these areas can be made to our current implementation of the CSM. The easiest improvement to implement would be to choose a method for evaluating integrals of the form (A11) which requires fewest sample points in the ω–k plane. Since our ultimate goal is to obtain a seismogram of a specified accuracy, the following questions regarding ω–k sampling should be investigated. Can a very sparse sampling along the real k-axis be used when $\mathrm{Im}(\omega)$ is large since the integrands are very smooth for large $\mathrm{Im}(\omega)$, or does the multiplication of the seismogram by $\exp[\mathrm{Im}(\omega)t]$ require a dense sampling of the smooth integrand to keep errors bounded? Should the sampling vary if we desire an accurate accelerogram rather than a displacement record? Should the sampling anticipate the high frequency taper applied to the seismogram spectra?

The CSM could be improved for large $\mathrm{Re}(\omega)$ by interchanging the collocation technique with other techniques for solving the boundary value problem when appropriate. For example, when $\mathrm{Re}(\nu_\alpha)$ and $\mathrm{Re}(\nu_\beta)$ are small the matrix Γ_i in (43) could be the exact propagator matrix (i.e. the layer matrix) if α, β and ρ are constant for $z_i \leqslant z \leqslant z_{i+1}$ and Γ_i could be an asymptotic approximation if α, β and ρ vary gradually with depth and the approximation is valid between z_i and z_{i+1}, as in Cormier (1980). On the other hand, the collocation approximation to Γ_i could be used near turning points, in regions of large velocity gradient, or when ν_α or ν_β have significant real parts.

In addition, for large $\mathrm{Re}(\omega)$ and k, additional savings might be achieved by factoring ω out of the A matrix, as advocated by Kennett & Kerry (1979), and working on a fixed set of slownesses for all frequencies. In order to avoid redundant calculation, one would also have to use the same mesh in z for all frequencies. When using the collocation technique this would probably be done economically for evanescent solutions but might not be appropriate for oscillatory solutions.

Since we have not yet attempted to optimize the CSM with respect either to sampling in the ω–k plane or to efficiency at high frequencies, we cannot say with certainty how

economical the CSM will ultimately be in any particular application. However, it is clear that the current implementation of the CSM is better suited to some applications than others.

The current version of the CSM is probably most useful for two classes of problems, those involving extended seismic sources and those which for some reason are so pathological that they elude solution by other less general methods. For example, consider the problem of calculating ground motions in a region from 0 to 100 km epicentral distance from a magnitude 6.5 earthquake having surface rupture and a 10 km hypocentral depth. In this case one needs Green's functions for sources at a wide range of depths, which the CSM automatically yields if one saves the results for all mesh points. Any particular observation location may simultaneously receive all types of near-field and far-field body and surface waves, and, as long as the ω–k window is large enough, the CSM cheerfully disgorges all these waves with very little user intervention.

In addition, due to its generality the CSM may be used for problems involving frequency-dependent Q, low-velocity zones, strong velocity-gradient regions, and other situations where many common approximations, such as the WKBJ approximation, break down. On the other hand, use of the CSM for point sources is generally a bit of overkill and is clearly not warranted if the Earth response is well approximated by surface waves or a small number of body waves, particularly at high frequencies.

Acknowledgments

We would like to thank Allen Olson for numerous helpful discussions, and for providing notes about the DWFE method and a working version of his code. Our work was initiated during the Coyote Lake Workshop organized by W. H. K. Lee.

References

Aki, K. & Richards, P. G., 1980. *Quantitative Seismology,* **1,** W. H. Freeman, San Francisco.

Alekseev, A. S. & Mikhailenko, B. G., 1980. The solution of the dynamic problem of elastic wave propagation in inhomogeneous media by a combination of partial separation of variables and finite difference methods, *J. Geophys.,* **48,** 161–172.

Ascher, U. & Weiss, R., 1983. Collocation for singular perturbation problems I: first order systems with constant coefficients, *J. Soc. ind. appl. Math. numer. Anal.,* **20,** 537–549.

Ascher, U. & Weiss, R., 1982. Collocation for singular perturbation problems II: linear first order systems without turning points, *Techn. Rep. 82-4,* Department of Computer Science, University of British Columbia, Vancouver, Canada.

Ben-Menahem, A. & Singh, S. J., 1981. *Seismic Waves and Sources,* Springer-Verlag, New York.

Borcherdt, R. D., 1977. Reflection and refraction of type II *S* waves in elastic and anelastic media, *Bull. seism. Soc. Am.,* **67,** 43–67.

Cormier, V. F., 1980. The synthesis of complete seismograms in an earth model specified by radially inhomogeneous layers, *Bull. seism. Soc. Am.,* **70,** 691–716.

de Boor, C. & Weiss, R., 1980. SOLVEBLOK: a package for solving almost block diagonal linear systems, *ACM Trans. Math. Software,* **6,** 80–87.

Fuchs, K. & Müller, G., 1971. Computation of synthetic seismograms with the reflectivity method and comparison with observations, *Geophys. J. R. astr. Soc.,* **23,** 417–433.

Hartzell, S. H. & Helmberger, D. V., 1982. Strong motion modelling of the Imperial Valley earthquake of 1979, *Bull. seism. Soc. Am.,* **72,** 571–596.

Harvey, D. J., 1981. Seismogram synthesis using normal mode superposition: the locked mode approximation, *Geophys. J. R. astr. Soc.,* **66,** 37–69.

Keller, H. B., 1976. Numerical solutions of two point boundary value problems, *SIAM series in Applied Mathematics 24.*

Kennett, B. L. N., 1975. The effects of attenuation on seismograms, *Bull. seism. Soc. Am.,* **65,** 1643–1651.

Kennett, B. L. N. & Kerry, N. J., 1979. Seismic waves in a stratified half space, *Geophys. J. R. astr. Soc.*, **57**, 557–583.

Olson, A. H., Orcutt, J. A. & Frazier, G. A., 1983. The discrete wavenumber/finite element method for synthetic seismograms, *Geophys. J. R. astr. Soc.*, submitted.

Phinney, R. A., 1965. Theoretical calculations of the spectra of first arrivals in layered elastic mediums, *J. geophys. Res.*, **70**, 5107–5123.

Richards, P. G., 1981. Basic results in wave attenuation – a surprise and a caveat, *Eos, Trans. Am. Geophys. Un.*, **62**, 959.

Takeuchi, H. & Saito, M., 1972. Seismic surface waves, in *Methods of Computational Physics*, **11**, ed. Bolt, B. A., Academic Press, New York.

Weiss, R., 1974. The application of implicit Runge-Kutta and collocation methods to boundary-value problems, *Math. Comp.*, **28**, 449–464.

Wiggins, R. A., 1976. A fast, new computational algorithm for free oscillations and surface waves, *Geophys. J. R. astr. Soc.*, **47**, 135–150.

Appendix A: integral transforms

In this section we define the various integral transforms used, and introduce some notation. Following Takeuchi & Saito (1972) and Ben-Menahem & Singh (1981), we present the orthogonal vector functions **R**, **S** and **T** employed in spatial transforms, defined by

$$\begin{aligned}
\mathbf{R}_k^m(r,\phi) &= Y(k,m,r,\phi)\,\hat{\mathbf{z}} \\
\mathbf{S}_k^m(r,\phi) &= \frac{1}{k}\frac{\partial Y}{\partial r}\hat{\mathbf{r}} + \frac{1}{kr}\frac{\partial Y}{\partial \phi}\hat{\boldsymbol{\phi}} \\
\mathbf{T}_k^m(r,\phi) &= -\hat{\mathbf{z}}\times\mathbf{S}_k^m = \frac{1}{kr}\frac{\partial Y}{\partial \phi}\hat{\mathbf{r}} - \frac{1}{k}\frac{\partial Y}{\partial r}\hat{\boldsymbol{\phi}}
\end{aligned} \tag{A1}$$

where $\hat{\mathbf{r}}$, $\hat{\boldsymbol{\phi}}$, and $\hat{\mathbf{z}}$ are unit vectors in a cylindrical coordinate system, and where

$$Y(k,m,r,\phi) = J_m(kr)\exp(im\phi), \qquad m = 0, \pm 1, \pm 2, \ldots$$

Note that m is a discrete variable while the others are continuous.

If we define the following inner product

$$(\mathbf{a},\mathbf{b}) = \int_0^{2\pi}\int_0^{\infty} r\mathbf{a}\cdot\mathbf{b}^* dr\, d\phi \tag{A2}$$

where the asterisk denotes complex conjugate, then **R**, **S** and **T** satisfy the following orthogonality relations

$$\begin{aligned}
(\mathbf{R}_k^m, \mathbf{R}_l^n) = (\mathbf{S}_k^m, \mathbf{S}_l^n) = (\mathbf{T}_k^m, \mathbf{T}_l^n) &= \frac{2\pi}{\sqrt{kl}}\,\delta_{mn}\delta(k-l) \\
(\mathbf{R}_k^m, \mathbf{S}_l^n) = (\mathbf{R}_k^m, \mathbf{T}_l^n) = (\mathbf{S}_k^m, \mathbf{T}_l^n) &= 0.
\end{aligned} \tag{A3}$$

Since **R**, **S** and **T** are orthogonal, any vector function **v** of r, ϕ and z may be written as a linear combination of them:

$$\mathbf{v}(r,\phi,z) = \sum_{m=-\infty}^{\infty}\int_0^{\infty}\frac{k}{2\pi}\left[A(k,m,z)\,\mathbf{R}_k^m(r,\phi) + B\mathbf{S}_k^m + C\mathbf{T}_k^m\right]dk \tag{A4}$$

where

$$A(k, m, z) = (\mathbf{v}, \mathbf{R}_k^m)$$
$$B(k, m, z) = (\mathbf{v}, \mathbf{S}_k^m) \tag{A5}$$
$$C(k, m, z) = (\mathbf{v}, \mathbf{T}_k^m).$$

For temporal transforms we use the Fourier transform pair,

$$\bar{f}(\omega) = \int_{-\infty}^{\infty} \exp(i\omega t) f(t)\, dt$$
$$f(t) = \frac{1}{2\pi} \int_{-\infty}^{\infty} \exp(-i\omega t)\, \bar{f}(\omega)\, d\omega \tag{A6}$$

where ω may be complex and $\mathrm{Im}(\omega) \geqslant 0$. Note the sign convention employed. With this definition of the Fourier transform, we may expand any vector function of both space and time by

$$\mathbf{v}(r, \phi, z, t) = \frac{1}{2\pi} \int_{-\infty}^{\infty} \exp(-i\omega t) \sum_m \int_0^{\infty} \frac{k}{2\pi} [A\mathbf{R}_k^m + B\mathbf{S}_k^m + C\mathbf{T}_k^m]\, dk\, d\omega \tag{A7}$$

or

$$\bar{\mathbf{v}}(r, \phi, z, \omega) = \sum_m \int_0^{\infty} \frac{k}{2\pi} [A\mathbf{R}_k^m + B\mathbf{S}_k^m + C\mathbf{T}_k^m]\, dk. \tag{A8}$$

In instances when A, B and C are non-zero for only a few values of m, the following notation becomes useful. Define $\tilde{f}$ by

$$f = \frac{1}{2\pi} \int_{-\infty}^{\infty} \exp(-i\omega t) \int_0^{\infty} \frac{k}{2\pi} \tilde{f}\, dk\, d\omega. \tag{A9}$$

With this definition, writing (A7) is similar to writing

$$\tilde{\mathbf{v}}^m = A\mathbf{R}_k^m + B\mathbf{S}_k^m + C\mathbf{T}_k^m. \tag{A10}$$

The efficient evaluation of expressions like (A9) is still a matter under investigation by us and others. For the examples shown in this paper we have used an extension of the discrete-wavenumber summation, introduced by Alekseev & Mikhailenko (1980) and Olson *et al.* (1983), in which an integral of the form

$$f(r) = \int_0^{\infty} kg(k) J_i(kr)\, dk, \qquad i = 0, 1 \tag{A11}$$

is replaced by the sum

$$f(r) = \sum_{n=N_1}^{N_2} c_n g(k_n) J_i(k_n r) \tag{A12}$$

$$c_n = \frac{2}{R^2 [J_0(k_n R)]^2}; \quad J_1(k_n R) = 0. \tag{A13}$$

As pointed out by the previous authors, the physical effect of this substitution is to introduce an artificial boundary at $r = R$, and hence R must be chosen sufficiently large so that waves reflected from this boundary arrive at the receiver locations after the last outgoing signal of interest. In addition, note that the k_n in (A13) are the roots of $J_1(k_n R)$ for both $i = 0$ and 1 in (A11). This easily derived extension of the previous authors' work cuts in half the number of sample points required in the k domain. The choice of N_1 and N_2 in (A12) is made by determining the portion of the ω–k plane for which the seismic response is desired. By allowing N_1 and N_2 to be functions of ω, phase velocity filtering of the theoretical seismograms is easily performed.

The inverse Fourier transform is performed using a standard FFT and subsequent multiplication of the time domain signal by the growing exponential $\exp[\mathrm{Im}(\omega)t]$ to remove the effect of the complex frequency. This convenient trick, introduced by Phinney (1965) simultaneously smooths the integrand and diminishes the wrap-around problem inherent in the use of an FFT.

Like the DWFE method, the computation time required by this version of the CSM is roughly proportional to the cube of the desired frequency bandwidth. Since equally spaced frequencies are required by the FFT, the number of frequencies needed grows linearly with bandwidth. Similarly, if lines of constant phase velocity are used to bound the region of integration in the ω–k plane, the required number of wavenumbers $(N_2 - N_1)$ rises linearly with ω. Finally, the number of mesh points required to solve the P–SV and SH equations is roughly proportional to frequency.